# Photoactivatable GFP resolves *Drosophila* mesoderm migration behaviour

**Michael J. Murray and Robert Saint***

Mesoderm migration is a pivotal event in the early embryonic development of animals. One of the best-studied examples occurs during *Drosophila* gastrulation. Here, mesodermal cells invaginate, undergo an epithelial-to-mesenchymal transition (EMT), and spread out dorsally over the inner surface of the ectoderm. Although several genes required for spreading have been identified, our inability to visualise mesodermal cells in living embryos has left us to speculate about the cell rearrangements involved. Several mechanisms, such as chemotaxis towards a dorsally expressed attractant, differential affinity between mesodermal cells and the ectoderm, and convergent extension, have been proposed. Here we resolve the behaviour of *Drosophila* mesodermal cells in live embryos using photoactivatable-GFP fused to α-Tubulin (PAGFP-Tub). By photoactivating presumptive mesodermal cells before gastrulation, we could observe their migration over non-fluorescent ectodermal cells. We show that the outermost (outer) cells, which are in contact with the ectoderm, migrate dorsolaterally as a group but can be overtaken by more internal (inner) cells. Using laser-photoactivation of individual cells, we then show that inner cells adjacent to the centre of the furrow migrate dorsolaterally away from the midline to reach dorsal positions, while cells at the centre of the furrow disperse randomly across the mesoderm, before intercalating with outer cells. These movements are dependent on the FGF receptor Heartless. The results indicate that chemotactic movement and differential affinity are the primary drivers of mesodermal cell spreading. These characterisations pave the way for a more detailed analysis of gene function during early mesoderm development.

KEY WORDS: Mesoderm, Cell migration, *Drosophila*, Photoactivatable GFP

## INTRODUCTION

Early in embryogenesis a complex series of cell and tissue movements, termed gastrulation, transform a simple arrangement of cells, commonly a topologically two-dimensional epithelium, into a complex three-dimensional body plan consisting of three primary germ layers: ectoderm, mesoderm and endoderm (Leptin, 2005). Although details vary between species, the formation of the mesoderm typically involves cells of the primitive ectoderm undergoing an epithelial-to-mesenchymal transition (EMT), moving internally and spreading out over the basal surface of the ectoderm. In *Drosophila*, presumptive mesodermal cells are internalised through the formation of a ventral furrow, undergo an EMT and then spread out over the ectoderm to form a monolayer (Stathopoulos and Levine, 2004; Wilson and Leptin, 2000). In spite of the central importance of this process, difficulties in visualising the mesoderm in living embryos, particularly in higher vertebrates and in *Drosophila*, has meant that our understanding of the cellular behaviour during mesoderm migration/spreading is limited.

In *Drosophila*, although several genes required for spreading have been identified, including the FGF receptor *heartless* (*htl*) (Beiman et al., 1996; Gisselbrecht et al., 1996), its putative ligands *thisbe* (*fgf8-like-1*) and *pyramus* (*fgf8-like-2*) (Gryzik and Muller, 2004; Stathopoulos et al., 2004), *sugarless* and *sulfateless* (Lin et al., 1999), *downstream of FGF receptor* (*dof*; also known as *stumps* and *heartbroken* – FlyBase) (Michelson et al., 1998; Vincent et al., 1998; Imam et al., 1999), and the Rho guanine nucleotide exchange factor *pebble* (Schumacher et al., 2004; Smallhorn et al., 2004), the manner

in which the monolayer is achieved is unknown. Several mechanisms have been proposed (Wilson and Leptin, 2000) (Fig. 1). In the chemotaxis model, expression of a chemoattractant in the dorsal part of the ectoderm induces mesodermal cells to migrate dorsally. In support of this model, mesodermal cells express Htl, while the ectodermal cells express Thisbe and Pyramus (Gryzik and Muller, 2004; Stathopoulos et al., 2004). In the differential affinity model, mesodermal cells have more affinity for the ectoderm than for each other and seek to maximise their contact with the ectoderm. In this model, activation of Htl would simply impart a degree of motility to cells, allowing inner cells to move over and in between existing outer cells until they were able to find contact with the ectoderm. In the convergent extension model, inner and outer cells move towards each other and intercalate, resulting in a net, lateral spreading of the tissue.

To better understand mesodermal cell behaviour during spreading, and to test the predictions of these models we wished to visualise mesodermal cells in living embryos using a fluorescent protein such as GFP. Regulatory sequences of genes specific to the mesoderm, such as *twist*, have been used previously to express cell shape markers to characterise mesoderm cell morphology (Schumacher et al., 2004; Smallhorn et al., 2004). However, due to the maturation time for GFP and the high levels of expression required to clearly image internal tissues, we found this approach to be impractical for live imaging of early mesodermal events (data not shown). In this paper we have utilised an alternative approach using photoactivatable GFP (PAGFP) (Patterson and Lippincott-Schwartz, 2002), a variant of wild-type GFP which, when activated by short wavelength light, exhibits a 100-fold increase in absorption at 488 nm.

Here we have expressed PAGFP ubiquitously in early embryos, allowing us to photoactivate presumptive mesodermal cells before they internalise, and subsequently view them migrating over non-photoactivated ectodermal cells. Taking advantage of the versatility

The ARC Special Research Centre for the Molecular Genetics of Development and Molecular Genetics and Evolution Group, Research School of Biological Sciences, The Australian National University, Canberra, ACT, 2601, Australia.

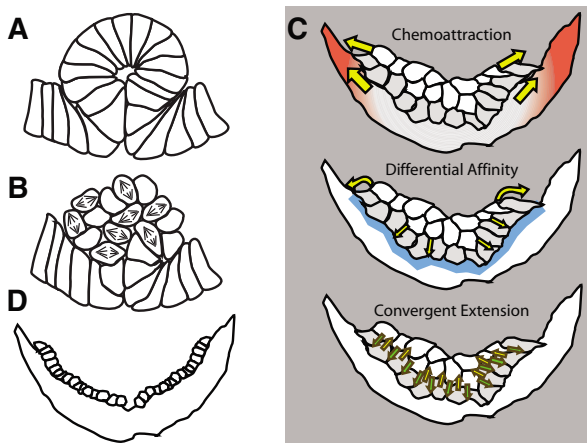*Author for correspondence (e-mail: robert.saint@anu.edu.au)

**Fig. 1. Models for mesoderm spreading in *Drosophila*.**
(**A**) Following invagination, the mesoderm forms an epithelial tube.
(**B**) The cells then undergo an EMT and divide once. (**C**) The
mesodermal cells then collapse down onto the ectoderm and begin to
spread out. We notionally divide cells into outer cells adjacent to the
ectoderm (grey) and inner cells (white). Three possible cellular
mechanisms for spreading are depicted [adapted from Wilson and
Leptin (Wilson and Leptin, 2000)]. In the Chemotaxis model, a
chemoattractant emanating from the dorsal part of the ectoderm (red)
attracts mesodermal cells dorsally. In the Differential Affinity model
mesodermal cells have more affinity for the ectoderm (blue) than for
each other, and seek to maximise their contact with the ectoderm. In
this model, activation of the FGF receptor Htl would simply impart a
degree of motility to cells allowing inner cells to move over, and in
between, existing outer cells until they were able to find contact with
the ectoderm. In the Convergent Extension model, inner and outer cells
move towards each other (arrows) and intercalate, resulting in a net,
lateral spreading of the tissue. (**D**) Eventually the mesoderm forms a
single layer of cells.

of PAGFP, we have been able to photoactivate and visualise the
movements of an entire section of mesoderm, as well as track the
fate of small numbers of cells using region-of-interest laser
photoactivation. We show that mesodermal cells initially in contact
with the ectoderm migrate dorsolaterally in concert with their
neighbours, while more internal cells are able to move over these
outer cells to arrive at the ectoderm in more dorsal positions. The
results broaden our understanding of mesoderm migration in general
and provide a basis on which to further understand the genetic
regulation of early mesoderm development in *Drosophila*.

## MATERIALS AND METHODS
### Molecular biology
PAGFP including an A206K mutation to reduce formation of dimers (G.
Patterson, personal communication) (Zacharias et al., 2002), was PCR
amplified and cloned into the *Eco*RI and *Not*I sites of the pENTR3C vector
(Invitrogen) to make pENT-PAGFP. α-Tubulin84B was PCR amplified from
fly genomic DNA using primers CGTGCTGTACAAGTACCGTGAATG-
TATCTC and GAATGCGGCCGCTTAGTACTCCTCAGC, digested with
*Bsr*GI and *Not*I and cloned into pENT-PAGFP to make pENT-PAGFP-
αTub84B. The insert was then transferred into a UASp destination vector
(cloning details available on request), and transformed into flies by standard
methods.

### Fly stocks
Fly stocks used in this study were *twist::CD2* (Bloomington), *pCOG-
Gal4VP16; NGT40; nanos-Gal4VP16* (Grieder et al., 2000), *htl$^{AB42}$/TM3,ftz-
lacZ* (Bloomington), *UASp-PAGFP-αTub84B* (this study) and *htl$^{AB42}$,UASp-
PAGFP-αTub84B/TM3,ftz-lacZ*. To obtain early embryos expressing high

levels of PAGFP-Tub, we crossed females of genotype *COG-
Gal4VP16/+;NGT40/+;nanos-Gal4VP16/UASp-PAGFP-αTub84B* to
*UASp-PAGFP-αTub84B* homozygous males. For analysis of *htl*
mutants, we crossed females of genotype *COG-Gal4VP16/+;NGT40/+;nanos-
Gal4VP16/htl$^{AB42}$,UASp-PAGFP-αTub84B* to *htl$^{AB42}$,UASp-PAGFP-
αTub84B/TM3,ftz-lacZ* males, and identified *htl* mutants by their failure to
form a monolayer. Tests using the *htl$^{AB42}$/TM3,ftz-lacZ* stock demonstrated a
clear qualitative difference between *htl$^{AB42}$/htl$^{AB42}$* embryos and control
embryos (i.e. *htl$^{AB42}$/+* and *+/+*) in their ability to achieve a clear monolayer
by 90 minutes post-gastrulation (data not shown).

### Photoactivation protocols
For whole-mesoderm observations, embryos were dechorionated and
approximately eight to ten pre-gastrulation embryos were transferred to a
coverslip coated with rubber cement (Chiaro), and immediately covered with
liquid paraffin. Embryos were then visualised under a 40× objective and
exposed for 1 second with the 405/20 nm light. They were then monitored
with 1 second exposures using a FITC filter set, until the onset of furrowing
was detected, at which point a 100× objective was used to expose a small
patch of presumptive mesoderm (approximately 10-12 cells in diameter) to
405/20 nm critical illumination light for 60 seconds. During this period the
focal plane was gradually changed to ensure all parts of the cells received
strong focussed light.

To ensure that photoactivated cells remained on the ventral side while
germ band extension was proceeding, we restricted photoactivation to cells
in the anterior half of the embryo, but posterior to the cephalic furrow.

To label small groups of cells we utilised region-of-interest activation on
a confocal microscope. Embryos were monitored using periodic scanning
with a 488 nm laser at 1-minute intervals until the onset of gastrulation was
detected. We then zoomed in by a factor of approximately 16, drew a polygon
around one or two cells of interest and scanned with UV 351 and 364 nm laser
lines at 200 Hz two to four times. Typically this resulted in strong
photoactivation of the outlined cell(s) and weaker activation of adjacent cells.

### Imaging protocols
Time-lapse sequences were collected on an inverted Leica confocal system,
with room temperature maintained at approximately 25°C. The images are
a compromise between the conflicting requirements of good image quality,
high temporal resolution and low photobleaching. As image quality
increases (e.g. via high spatial resolution 1024×1024, high z resolution, and
high laser intensity) so too does the degree of photobleaching of the
specimen. In addition, higher image resolution and Kalman averaging scans,
require a longer time to capture the z-series and therefore lowers temporal
resolution. The best compromise was a 3 μm z-series of 512×512 images
with three Kalman averages, and an interframe interval of 2 minutes. The
range of z-sections was also limited to encompass only the mesoderm to
minimize photobleaching and allow for more rapid sampling. The number
of z-slices was between 5 and 15 at the start of time-lapse sequences but
could increase to 21 by the end of the sequences as the mesoderm reached
increasingly dorsal positions and the mesoderm encompassed a greater
three-dimensional range.

### Data analysis
The whole mesoderm analyses presented here are based on 13 time-lapse
sequences that clearly showed the developmental events under analysis. We
excluded sequences in which: (1) the image quality was too poor; (2) the
embryo rolled; (3) the embryo desiccated; (4) there was a clear mitotic delay.
In this last category (*n*=4) the first mitotic wave, which normally occurs
within 5-15 minutes of the EMT, was delayed, occurring 30-40 minutes after
the EMT when the mesoderm was already migrating. In control embryos
staged to be midway through the migration period, 30-45 minutes after
gastrulation (*n*=12), we never observed more than a few cells undergoing
mitosis. We therefore excluded these sequences from analysis in spite of the
fact that the mesodermal cells appeared otherwise healthy and spread into a
monolayer.

To determine the normal sequence and timing of mesodermal events we
dechorionated twist::CD2 embryos and monitored them in a 25°C room on
a dissecting microscope until gastrulation was detected, and then aged them
for a given period of time. Embryos were then fixed (4% formaldehyde in

PBS) for 20-30 minutes and stained for CD2 and DNA, using Mouse-anti-RAT-CD2 (Serotec) at 1:100, goat anti-mouse Alexa 488 (1:200; Molecular Probes) and Hoechst 33258 (1:200; Molecular Probes).

Mesodermal cells first began to enter mitosis at 10 minutes ($n=9$), and by 20 minutes ($n=5$) the majority of cells were dividing. By 30 minutes ($n=7$) mitosis was essentially finished, with only isolated cells still dividing. No cells were dividing at 45 minutes ($n=5$). At 50 minutes ($n=5$) the second wave of division had begun, and by 60 minutes ($n=4$) was still occurring. By 80 minutes ($n=4$) divisions had again finished. Thus the timing of the first mitotic wave in time-lapse sequences at 30 minutes was delayed by approximately 10 minutes with respect to control embryos, but the period between the first and second waves of division of ~40 minutes was similar to control embryos. This initial delay is most likely due to the relatively cool temperature (~21-22°C) in the room in which whole mesoderm photoactivation took place. Once embryos had been transferred to the 25°C confocal room for time-lapse acquisition, developmental rates became comparable to control rates.

### Immunostaining of photoactivated embryos

Following photoactivation, embryos were removed from the liquid paraffin with a paintbrush, placed on an apple-juice agar plate and then gently moved around on the agar to reduce the amount of oil and glue remaining on the embryo. In the case of the IM/IL cell migration experiments (Fig. 8), embryos were aged to 90 minutes post-gastrulation at 25°C, or in the case of the embryos in Figs 6 and 7 processed immediately. Embryos were then fixed and cracked, rinsed once in methanol, three times in PBS+0.1% Triton X-100, immunostained over a period of two hours with Rb-anti-Twist (1:200) (a gift from M. Leptin, Institute of Genetics, University of Cologne, Germany) or BP106 (anti-Neurotactin, Developmental Studies Hybridoma Bank) and goat anti-rat Cy5 (Jackson ImmunoResearch), cleared and immediately imaged using confocal microscopy. The position of IM/IL cell clones within the mesoderm was quantified by measuring the distance from the midline to each cell along a path that followed the contours of the monolayer. Distances were normalised as a fraction of the total extent of the mesoderm in that section of the embryo containing the clone.

## RESULTS

### PAGFP-α-Tubulin as an in vivo marker for cell shape and division

We fused PAGFP to α-Tubulin84B (PAGFP-Tub), so that we could visualise the two rounds of division that occur during spreading, and expressed it in early embryos (see Materials and methods). These

embryos developed normally and produced viable and fertile adults. PAGFP-Tub was faintly fluorescent with FITC/488 nm filter sets before photoactivation and was easily photoactivated to strong fluorescence using either Hg lamp light passed through a 405/20 nm excitation filter (Fig. 2A), or UV laser illumination on a confocal microscope (Fig. 2B,C).

In interphase cells, photoactivated PAGFP-Tub localised to the cytoplasm and was excluded from the nucleus, allowing overall cell morphology to be visualised (Fig. 2D). As cells progressed through mitosis, PAGFP-Tub first localised strongly at the spindle poles, then moved into the region of the nucleus, presumably as nuclear envelope breakdown occurred. It then localised to the mitotic spindle, central spindle and was eventually excluded from the nucleus as the daughter cells again entered interphase (Fig. 2D). Thus PAGFP-Tub localises as expected for a functional Tubulin molecule and provides a marker for cell shape and the progression of division.

### Photoactivation of PAGFP-Tub during gastrulation permits visualisation of the development of the mesoderm

To robustly label the entire mesoderm over several segments, we exposed a patch of the presumptive mesoderm to 405/20 nm Hg light for 60 seconds during gastrulation (Fig. 2E), and then transferred the embryo to a confocal microscope, where the fluorescently labelled mesoderm was clearly distinguishable from the unlabelled ectoderm (Fig. 2F,G). To capture the three-dimensional movements of the mesoderm, a z-series of 3 μm slices was collected at 2-minute intervals (see Materials and methods for details). These parameters provided sufficient spatial and temporal resolution to track individual cells for 2-3 hours, without significant photobleaching.

In the only published *Drosophila* PAGFP study (Post et al., 2005), it was reported that illumination with a 408 nm diode laser could prevent cells from dividing, independent of the presence of PAGFP proteins. In another study, in which PAGFP was used to track migrating cells in chick embryos, photoactivation with a 405 nm laser did not appear to affect cell viability or behaviour (Stark and Kulesa, 2005). In the movies analysed here, neither photoactivation with Hg 405/20 nm or UV laser light, nor the subsequent 488 nm
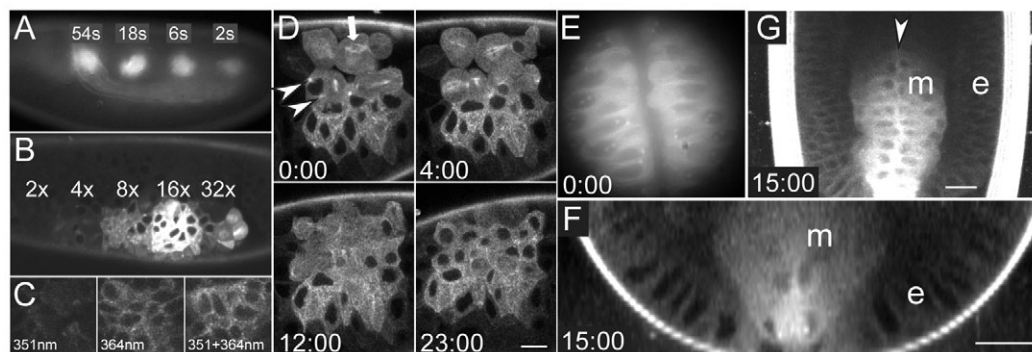


**Fig. 2. Photoactivation of PAGFP-αTub84D-expressing embryos.** Photoactivation in *Drosophila* embryos derived from *cogGAL4VP16/+;NGT40/+;nanos-GAL4VP16/UASp-PAGFP-αTub84D* females crossed to *UASp-PAGFP-αTub84D* homozygous males. (**A**) Photoactivation using Hg 405/20 nm light with a 60× objective. Post-activation fluorescence is approximately proportional to exposure time up to ~30 seconds. (**B**) Photoactivation using UV confocal laser light (both 351 and 364 nm) and a 63× objective. Fluorescence is approximately proportional to zoom level up to ~16×. (**C**) Photoactivation is possible with 351 nm UV laser light, stronger with 364 nm light, and strongest with both. (**D**) UV laser activation of a patch of epidermal cells. PAGFP-Tub is cytoplasmic, excluded from nuclei during interphase, and correctly localises to spindle poles (arrowheads) and mitotic spindle (arrow). (**E**) A gastrulating embryo after 60 seconds photoactivation using Hg 405/20 nm light. (**F,G**) z-series reconstruction (F) and z-projection (G) of same embryo imaged using confocal microscopy 15 minutes later, showing that the entire mesoderm is strongly labelled and easily distinguishable from the ectoderm. Scale bars: 10 μm in D; 20 μm in F-G. e, ectoderm; m, mesoderm.

**Fig. 3. Overview of mesoderm development in *Drosophila*.** Typical time-lapse sequence of an embryo with three to four segments of photoactivated mesoderm showing cells undergoing two divisions as they spread out into a monolayer (see Movie 1 in the supplementary material). (**A**) At 15 minutes post-gastrulation, the mesoderm shows a medial seam (arrowhead), indicating that the invaginated mesoderm is still arranged as an epithelial tube. (**B**) By 33 minutes, the EMT has occurred and the cells undergo a synchronous division, as evidenced by the appearance of mitotic spindle poles (arrowheads) and spindles (arrows). (**C**) At 1:03, the cells have re-entered interphase and are migrating out over the ectoderm. (**D**) At 1:19, the second division is in progress (arrows indicate spindles). During this division the mesoderm rapidly extends laterally. (**E,F**) By 2:15 the monolayer has been achieved and the embryo (E) shows a similar segmentally repeated striped pattern to a control embryo (F) (*twist::CD2*) (arrowheads). The segmentally repeated variation in brightness is due to the changing thickness of the epidermal/neural tissue, which attenuates the signal from the photoactivated mesoderm (data not shown). (**G,H**) z-series reconstruction at the end of time-lapse acquisition (G), showing that the mesoderm has adopted the typical monolayer arrangement seen in fixed *twist::CD2* control embryos (H). Scale bars: 20 μm.
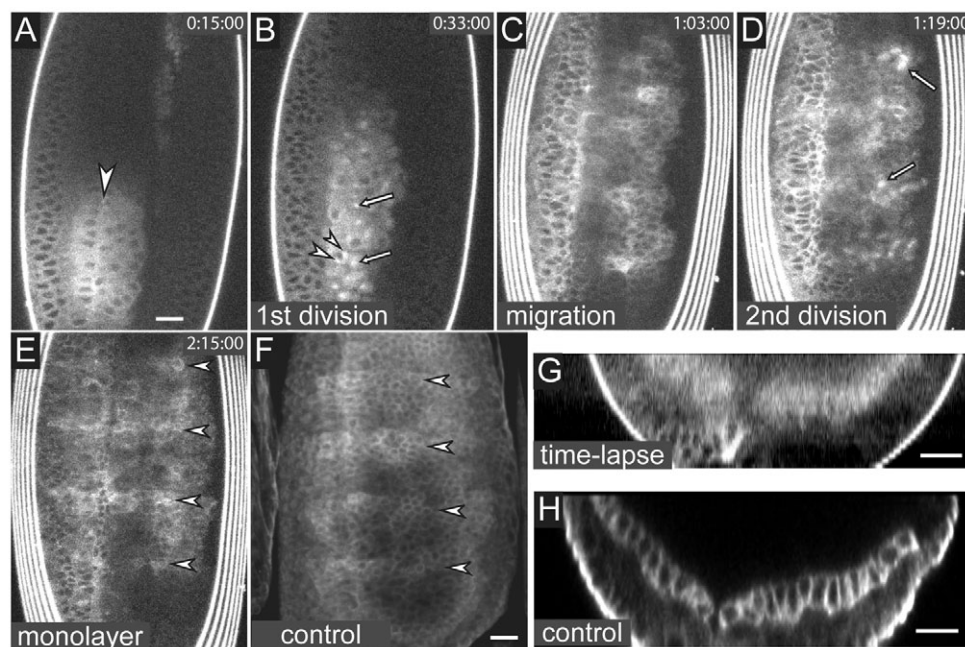
laser scanning, appeared to adversely affect development, based on the following observations: (1) gastrulating embryos photoactivated with 60 seconds Hg 405/20 nm light and then transferred to apple-juice agar plates (to prevent desiccation) hatched in all cases (*n*=19), indicating that the photoactivation protocol itself did not compromise embryo viability; (2) cells showed no evidence of undergoing cell death/fragmentation, underwent the expected rounds of cell division (Fig. 3B,D), adopted the expected morphologies during migration, correctly spread into a monolayer (Fig. 3G) and developed the expected patterns of segmentation (Fig. 3E); (3) embryos from time-lapse sequences (e.g. Figs 3, 4), that were allowed to continue development on apple-juice agar plates routinely hatched (*n*=6).

### Outer cells migrate laterally as a group
At the beginning of time-lapse sequences, approximately 15 minutes after the onset of gastrulation, the mesoderm was still in the form of an epithelial tube with a medial seam visible (Fig. 2G, Fig. 3A, arrowheads). This seam was lost as the cells underwent their EMT and then, shortly after, entered their first round of division at 29±9 minutes (s.d., *n*=13) post-gastrulation (Fig. 3B). Following this division, cells spread down onto the ectoderm and their nuclei again became clear as they entered interphase. Cells at the leading edge then adopted a migratory morphology (Fig. 3C, Fig. 4B).

At this stage there were three to four rows of outer cells on either side of the midline and a pool of inner cells. The outer cells clearly moved laterally over the ectoderm. For example, in Fig. 4B two cells were tracked over a period of 12 minutes, during which time they moved apart by 26 μm, a migration rate of approximately 1 μm/minute. As the cells migrated, other cells from more medial positions came to occupy the ectodermal positions that were thereby vacated (Fig. 4C,D, arrowheads). During this phase, the outer

migrating cells moved in concert with their immediate neighbours. For example, in Fig. 4E, as the marked cell (white dot) migrates, the adjacent cells (arrowheads) move with it.

### Inner cells can move over outer cells
Another behaviour that was commonly observed during this migration phase was that outer cells that were initially the most laterally placed were overtaken by inner cells. In Fig. 5, for example, cells marked by arrowheads migrated past the marked outer cell (white dot) that was initially the most laterally placed.

### Second mitosis and remodelling phase
The period of overtaking behaviour was shortly followed by a second round of division, which occurred at 70±12 minutes (s.d., *n*=11) post-gastrulation (Fig. 3D). This period of division was associated with a rapid lateral spreading of the mesoderm. The return to interphase was accompanied by some retraction/compaction of the mesoderm, suggesting that cells were re-adhering following mitosis. At this stage the mesoderm exhibited a segmentally repeated three-dimensional undulation, as seen in control embryos (Fig. 3E,F).

### Tracking inner cell migration using laser photoactivation
Our whole mesoderm observations indicated that some inner cells moved past outer cells to occupy more dorsolateral positions. Due to the inability of confocal microscopy to image more than a few cell diameters into the embryo, we were only able to detect these cells when they moved onto the ectoderm. To determine from where, in the invaginated epithelial tube, these cells originated, we used region-of-interest confocal UV laser scanning to photoactivate small subsets of mesodermal cells as the ventral furrow was forming and followed their subsequent migration.

**Fig. 4. Outer cells migrate dorsolaterally as a group.**
(**A**) Overview of a time-lapse sequence of a *Drosophila* embryo showing the initial epithelial tube (0:15:00), the EMT and first round of division (0:21:00), a migratory phase (0:31:00) and the onset of the second division (0:51:00). Lower panels give reconstructed cross-sectional views. (**B**) Following the first division, there are typically three to four rows of outer cells (i.e. cells that are in contact with the ectoderm) on either side of the midline, which move laterally over the ectoderm. Two cells on either side of the midline (white dots) are tracked for a period of 12 minutes (see Movie 2 in the supplementary material). This image (and C and E) show a single focal plane. Cells marked with a black dot have, by the last panel, moved dorsolaterally into a deeper focal plane (data not shown). (**C**) A more superficial focal plane showing the movement of outer cells in regions closer to the midline. The positions of the cells marked in B (white dots) (not visible in this focal plane) are here again depicted with white dots. The original location of these cells with respect to the ectoderm was tracked and is indicated with a black dot. As the marked cells move laterally, other cells (down arrowheads) move laterally to occupy the original positions of the marked cells on the ectoderm. Times are as in B. (**D**) A reconstructed cross-section showing the uneven nature of the ectodermal surface over which the cells migrate laterally. Rounded regions appear to be nascent neuroblasts (asterisks). The indicated cell (0:43:00, arrowhead) corresponds to the cell in C (arrowheads on right-hand side). Times are as in B. (**E**) Enlarged view of the sequence in B showing that the marked cell (white dot) maintains its relationship to neighbouring cells (arrowheads) during migration. The cell to the lower right of the marked cell moves into a deeper focal plane (data not shown). Scale bars: 20 μm.
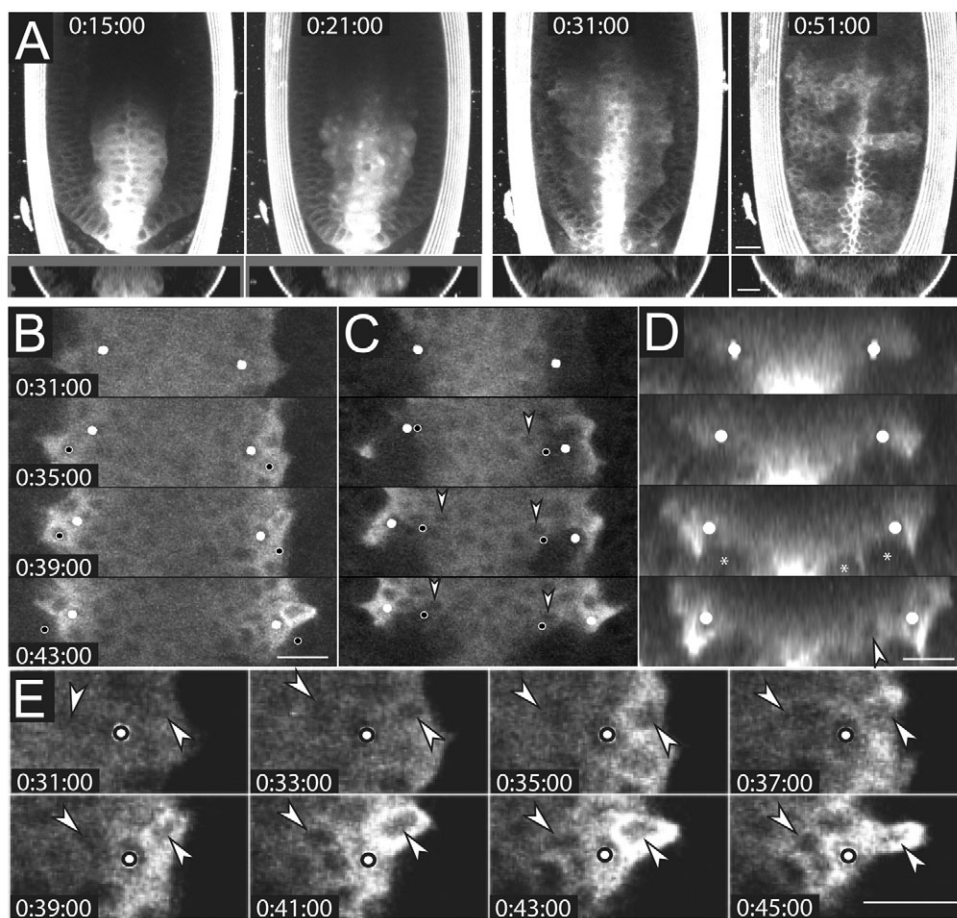
Pre-gastrulation embryos were monitored using 488 nm laser light to illuminate the faint, pre-activation levels of fluorescence (e.g. Fig. 6D). At the onset of furrowing, small groups of cells were photoactivated (see Materials and methods for details) either at the centre of the furrow [hereafter referred to as inner medial (IM) cells] (Fig. 6A), or immediately adjacent to the medial cells [hereafter: inner lateral (IL) cells] (Fig. 7A). The progress of IM and IL cells was then tracked by capturing z-series at 5-minute intervals. The cells were able to undergo their expected programmed divisions and remained motile, suggesting that UV irradiation did not compromise cell viability.

### Inner medial cell progeny become distributed over the entire mesoderm monolayer
As gastrulation proceeded and IM cells were internalised, their depth within the embryo quickly become too great for them to be visualised. Then, at 64±7 minutes (s.d., *n*=6), the IM cell progeny reappeared in a relatively short period (~10 minutes) (Fig. 6H-J). The number of cells was consistent with the original labelled cells having undergone two divisions. In Fig. 6, for example, the two cells that were strongly labelled result in about eight cells appearing later. The IM cell progeny were typically dispersed, distributed on either side of the midline, and could be scattered over the full extent of the mesoderm (Fig. 6J).

Based on the clarity of the cells and their z-depth into the embryo, these cells were judged to have reached the outer layer of the mesoderm, suggesting that the IM cell progeny had intercalated between existing outer cells. The timing of this event, around the time of the second mitosis, suggested that the ability of IM cells to find contact with the ectoderm increased during mitosis. Consistent with this idea, in fixed control embryos just before the second division (45 minutes post-gastrulation), isolated inner cells were often seen sitting on an outer monolayer (Fig. 6K).

### Inner lateral cell progeny move laterally as a group and reach a dorsolateral position
In contrast to IM cells, it was possible to track IL cell clusters, although initially appearing quite blurred because of their depth within the embryo. Following gastrulation, the cell clusters first translocated posteriorly through germ-band extension, and then, in all cases (*n*=9) moved laterally away from the midline as a group. At approximately 45 minutes post-gastrulation the progeny of the photoactivated IL cells became more distinct, consistent with them having contacted the ectoderm, and were positioned at the most dorsal region of the mesoderm (Fig. 7H). The cells were motile, and in some sequences were observed to divide at approximately 60 minutes.
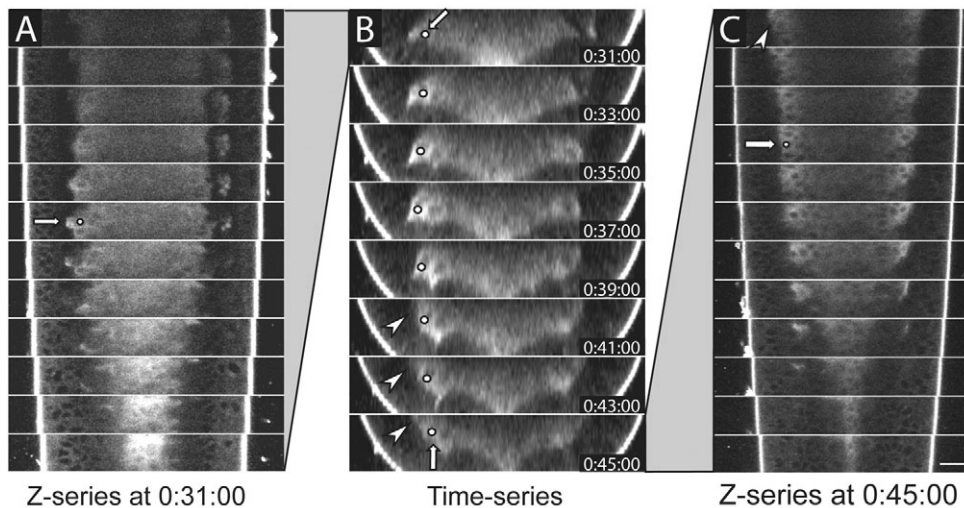
**Fig. 5. Inner cells can move over outer cells.** A time-lapse series of a *Drosophila* embryo showing inner cells (those not adjacent to the ectoderm) moving over outer cells (see Movie 3 in the supplementary material). (**A**) A 2 μm z-series at 0:31:00 showing a labelled cell (white dot and arrow) that is, at this time, the most laterally placed cell. (**B**) A reconstructed cross-sectional time-series in which the labelled cell (white dot and arrows) is overtaken by inner cells (arrowheads). (**C**) A z-series at end of the time-lapse showing that at deeper z-slices new cells (arrowhead) are now more dorsolaterally placed than the labelled cell (arrow). Scale bar: 20 μm.

In two cases, in addition to photoactivating IL cells we photoactivated cells adjacent and lateral to IL cells. Based on the typical number of cells in the invaginated epithelial tubes, we would expect these cells to be situated on the lateral side of the epithelial tube before the EMT, and hence likely to find themselves in contact with the ectoderm following the EMT and first division. We refer to these cells as outer lateral (OL) cells. In both cases the IL cell progeny ended up in a more dorsolateral position than the OL cell progeny (see Fig. S1 in the supplementary material). This again supports the idea that inner lateral cells migrate past outer cells.

## Analysis of IM and IL cell clone migration in fixed embryos

To extend our analysis of IM and IL cell migration we next took advantage of the fact that photoactivated PAGFP survives fixation. We photoactivated single IM and IL cells at gastrulation, and allowed the embryos to develop for 90 minutes, by which time the monolayer was established. Embryos were then fixed and immunostained for Twist (Fig. 8). In each case the labelled IM or IL cell had divided twice to produce a four-cell clone.
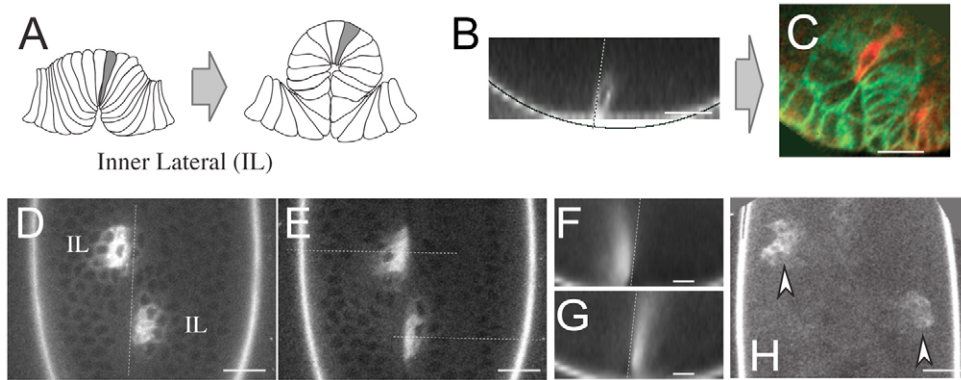
**Fig. 6. Inner medial cells become dispersed and intercalate towards the ectoderm.** (**A**) We define inner medial (IM) cells as cells at the centre of the furrow, which will be situated at the innermost point (top) of the invaginated epithelial tube (dark grey) after gastrulation. (**B**) Photoactivated IM cell at gastrulation. The midline is indicated by the radial line. (**C**) The same cell ~5 minutes later is now situated at the top of the invaginated epithelial tube. Photoactivated fluorescence (red), Neurotactin (green). (**D**) Before gastrulation, embryos were monitored using the low levels of pre-activation fluorescence until the onset of furrowing was detected. The furrow was first detected as a slight flattening at the anterior and posterior ends of the nascent furrow. (**E**) Two cells at the centre of the developing furrow were first
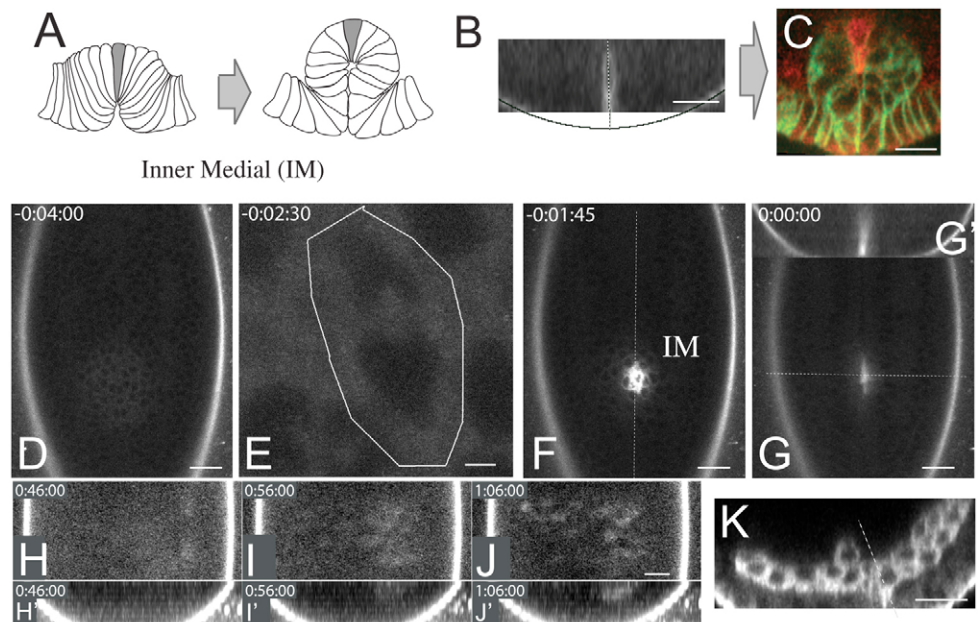


scanned with 488 nm laser at zoom ×14.5. A polygon was then drawn around them and they were scanned with the UV laser. (**F**) This resulted in the two cells being brightly labelled, with some neighbouring cells also being weakly labelled. The dotted line shows the midline. (**G,G′**) One minute 45 seconds later the furrow has formed and the photolabelled cells are internalised. This morphological stage is used as the zero time-point for all timings in movies. A reconstructed cross-section through the dotted line is shown in G′. (**H-J**) A time-lapse sequence at a constant focal plane showing the appearance of inner cell progeny at approximately 1 hour post-gastrulation. (**H′-J′**) Reconstructed cross-sections of z-series in upper panels. (H) At 0:46:00 the inner medial cell progeny are too internal to be detected. White blurred areas on the right are yolk. (I) At 0:56:00 minutes the inner medial cell progeny are first detected. (J) By 1:06:00 the cells are clearer, and are dispersed across the mesoderm. As seen in the reconstructed cross-section panel below, the cells are at a depth typical of cells adjacent to the ectoderm. (**K**) An isolated inner cell in a fixed control embryo shortly before the second division. Dotted line shows midline. Scale bars: 20 μm in B-D,F-K; 2 μm in E.

**Fig. 7. Inner lateral cells move as a group laterally to dorsolateral positions.** (**A**) We define inner lateral (IL) cells as cells adjacent to IM cells. (**B**) Photoactivated IL cell at gastrulation. The midline is indicated by the radial line. (**C**). The same cell ~5 minutes later is situated just to the right of the midline in the invaginated epithelial tube. Photoactivated fluorescence (red), Neurotactin (green). (**D**) Two IL clusters photoactivated on either side of the midline. (**E-G**) Time-point 0′ showing clusters internalising. Reconstructed cross-sections through the dotted lines are shown in F and G. (**H**) Following spreading, the two clusters have migrated to dorsolateral positions at opposite sides of the embryo (arrowheads). Dotted lines in B,D,F,G show the midline. Scale bars: 20 μm in B-E,H; 10 μm in F,G.

As in the time-lapse experiments, IM cell progeny were distributed across the full extent of the mesoderm (*n*=12) (Fig. 8A,B). In all cases the four IM cell progeny were grouped into two pairs of cells. Pairs were often separated by long distances and could occur on opposite sides of the midline. These pairs most likely represent sister cells resulting from the second division, suggesting that sister cells arising from the first division are able to migrate independently.

IL cell migration assayed using this approach also recapitulated the time-lapse results. In all cases (*n*=13) IL cell progeny clusters migrated away from the midline and ended up in the most dorsal half of the mesoderm (Fig. 8C,D). In approximately half of these cases the clone of cells extended to the dorsalmost edge of the mesoderm.

### IM and IL cell cluster migration depends on the FGF Receptor Heartless

To see if these movements were dependent on FGF signalling, we photoactivated IM and IL cells in $htl^{AB42}$ mutant embryos. IM cell progeny tended to remain in single clusters, as opposed to two pairs of cells, and in most cases (*n*=7/8) remained in the more medial half of the mesoderm. Similarly, in most cases (67%, *n*=12) IL cell progeny failed to migrate into the dorsalmost region of the mesoderm, but instead remained close to their initial position.

### DISCUSSION

Using a combination of whole mesoderm and single-cell photoactivation we have for the first time observed the combination of cell behaviours employed by *Drosophila* mesodermal cells to form a monolayer, providing insights into the mechanisms responsible for this important part of gastrulation. Our first observation was that outer cells moved dorsolaterally over the ectoderm. Although this is not unexpected, it nevertheless confirms a central prediction of the chemoattraction model: that cells migrate in a dorsolateral direction (Fig. 1C). Remarkably, we then observed that inner cells were able to overtake outer cells to achieve a more dorsal position. Single-cell labelling then showed that these inner cells were likely to have originated from a position adjacent to the centre of the ventral furrow. Significantly, IL cell progeny invariably moved away from the midline, suggesting that they receive a directional guidance cue from the dorsal region of the ectoderm, again consistent with a chemoattraction model.

A complication in the simple chemoattraction model is that the two likely chemoattractants, Pyr and Ths, are initially expressed in quite broad lateral domains (Gryzik and Muller, 2004; Stathopoulos et al., 2004). During mesoderm migration, however, *pyr* expression does become restricted to the more dorsal parts of the ectoderm, whereas *ths* is expressed in a complementary fashion in the ventral regions of the neurogenic ectoderm (Stathopoulos and Levine, 2004). It has been suggested that the two ligands may have different binding affinities, and that the refinement of Pyr expression to more dorsal positions could guide mesodermal cells dorsally (Stathopoulos and Levine, 2004). An alternative is that those regions of the ectoderm that are not yet covered with mesodermal cells, such as the dorsal ectoderm, are highly attractive to mesodermal cells simply because the FGF ligands that they are producing are not being bound and internalised by outer cells already in contact with the ectoderm.

An alternative to chemoattraction that has been suggested is that FGFR activation is permissive rather than instructive and simply imparts a degree of motility to cells, allowing them to disperse until they are able to contact the ectoderm (Wilson and Leptin, 2000). This motility, combined with a steric hindrance effect, in which cells tended to move into unoccupied territory, could theoretically achieve a monolayer in the absence of directional cues. We would expect, however, that if IL cell progeny were simply made motile and moved randomly, that cells adjacent to the midline would sometimes cross the midline to contact the ectoderm on the opposing side. This was never observed.

The movement of inner cells past the lateralmost outer cells is also consistent with the differential affinity model (Fig. 1C), according to which mesodermal cells form strong adhesions with the ectoderm. Cells not already in contact with the ectoderm would either intercalate between existing outer cells, or, as seen here, move past them. The fact that we do not observe intercalation suggests either that outer cells adhere strongly to the ectoderm and do not easily move apart, or, again, that outer cells are masking FGF produced in the ectoderm. If a differential affinity model is active, the most likely candidate adhesion molecules would be integrins, which are expressed at the interface of the mesoderm and ectoderm (Roote and Zusman, 1995) (data not shown), although there is, as yet, no published evidence for a functional role for integrins in this process.

DEVELOPMENT

**Fig. 8. Migration outcomes for inner medial and inner lateral cell clones.** IM and IL cells were photoactivated in control and *htl*[AB42] mutant *Drosophila* embryos (see Materials and methods for details) and development allowed to proceed until 90 minutes after gastrulation. The embryos were then fixed and immunostained for the mesoderm specific transcription factor Twist. By this stage, the monolayer was established and the photoactivated cells had divided twice to form clones of four cells. (**A,C,E,G**) Typical clones of photoactivated cells (red) within the mesoderm stained for Twist (green). (**B,D,F,H**) Schematics of IM/IL clone positions in control and *htl*[AB42] embryos. Positions within the monolayer were calculated as a fraction of the full extent of the mesoderm, and are depicted as grey circles at proportional positions within the black boxes. The mean extent of the mesderm in control (143±15 μm, s.d.) versus *htl*[AB42] (112±22 μm, s.d.) embryos is reflected by the width of the boxes. Boxes outlined in red correspond to the example embryos shown (A,C,E,G). (A) An IM clone
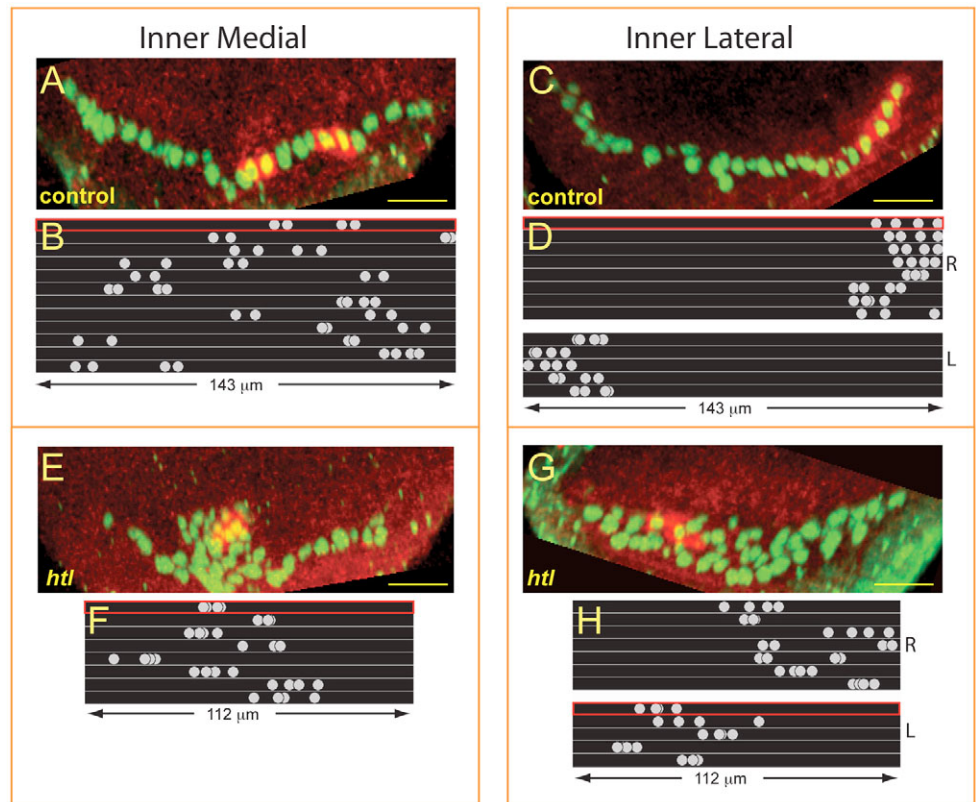


arranged as two pairs of cells within the mesoderm monolayer. (B) IM clones spanned the full extent of the mesoderm and were typically arranged as two pairs of cells. Pairs could be widely separated and located on opposite sides of the midline. (C) An IL cell, to the right of the midline, has produced a clone of cells at the right hand, dorsalmost part of the mesoderm. (D) IL clones in control embryos are grouped into those arising from IL cells initially located to the right of the midline (*n*=8) and those arising from IL cells to the left of the midline (*n*=5). In all cases, clones did not cross the midline and were positioned in the dorsal part of the mesoderm. (E) A *htl*[AB42] embryo in which the mesoderm has failed to spread into a monolayer. The clone of cells from an IM cell has failed to move away from the centre of the embryo. (F) IM clones in *htl*[AB42] embryos tended to remain fairly central, and did not separate into two distinct pairs. (G) An IL cell to the left of the midline in a *htl*[AB42] mutant, has produced a clone of cells that have not migrated out to the dorsal edge of the mesoderm. (H) IL clones in *htl*[AB42] embryos tended to stay on the same side of the midline as the progenitor cell, but did not usually reach the dorsalmost regions of the mesoderm. Scale bars: 20 μm.

During the initial migration of outer cells over the ectoderm we found that cells maintained their position relative to their immediate neighbours. This result supports the argument against the convergent extension model (Fig. 1C). If convergent extension was a primary driving force behind lateral spreading, one would expect to see widespread intercalation throughout the mesoderm as inner cells pushed in between existing outer cells. This was not observed, although we cannot rule out the possibility that some degree of intercalation does occur during this migration phase. Intercalation does, however, appear to play a part during the later stages of the formation of the monolayer, where we see IM cell progeny appearing at the ectoderm. The timing of this event, at around the time of the second mitosis, suggests that the sudden lateral spreading that accompanies the second mitotic wave may be due to the intercalation of a pool of inner cells. One possibility is that the adhesion between the mesodermal cells and the surrounding cells, both mesodermal and ectodermal, is decreased as they go through mitosis (Maddox and Burridge, 2003), permitting the inner cells access to their preferred position in association with the ectoderm. Thus, although a general convergent extension is not in evidence, intercalation does appear to contribute to mesoderm spreading.

On the basis of these observations, we propose the following model of mesoderm cell behaviour following ventral furrow formation, summarized in Fig. 9. Following the breakdown of the

epithelium, the first division results in a rapid spreading down onto the ectoderm, presumably due to decreased adhesion between mesodermal cells (Fig. 9A,B). Cells that are thereby placed in contact with the ectoderm start to polarise and proceed to migrate dorsolaterally as a group (Fig. 9C). Outer cells form a strong adhesive contact with the ectoderm, which prevents inner cells from intercalating between them and instead forces inner cells either to take up positions that outer cells vacate near the midline or move past them to more dorsal positions. Inner lateral cells receive a directional cue from the dorsal ectoderm guiding them laterally, over the outer cells. In this manner, by the time of the second mitosis the ectoderm is largely covered by mesodermal cells. Inner medial cell progeny that have failed to contact the ectoderm during the initial spreading are prevented from doing so by cells already strongly adhered to the ectoderm until the time of the second division. The second division then allows the remaining inner cells to contact the ectoderm (Fig. 9D). This intercalation produces a rapid lateral extension followed by a general retraction as the cells exit mitosis and re-establish adhesive contacts, with the ectoderm finally forming the monolayer.

The combination of behaviours we observe may represent the most efficient way to rapidly spread one tissue over another. The tendency for cells to migrate dorsolaterally helps to constantly make space for those cells placed nearer the midline. If cells that contacted the ectoderm never moved away, it would mean that internal cells
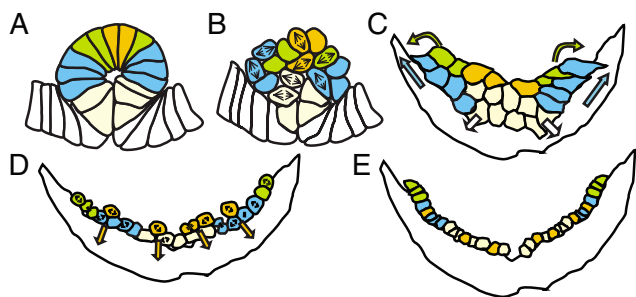
**Fig. 9. Model for mesodermal spreading in *Drosophila* embryos.**
(**A**) The invaginated epithelial tube before the EMT. (**B**) The mesodermal cells spread down onto the ectoderm as the EMT and first division occur. (**C**) Outer cells polarise and proceed to migrate dorsolaterally as a group (blue). As they move away, other cells take up their positions on the ectoderm (white arrows). Inner lateral cells (green) are attracted to the dorsal ectoderm and move over the outer cells. (**D**) During the second mitosis, inner medial cells (orange) that have failed to contact the mesoderm intercalate into the outer cell layer. (**E**) The monolayer is formed. See Discussion for details.

would have to travel further and further dorsally to find space on the ectoderm. In a similar manner, if chemotaxis towards a dorsally placed attractant was the only mechanism operating, one might expect that cells would continue moving dorsally, even if this resulted in an excess of cells in dorsal positions and a deficit closer to the midline. The tendency of mesodermal cells to develop and maintain a strong adhesive contact with the ectoderm would help ensure that all parts of the ectoderm remain covered. Finally, having a period of intercalation serves to give any remaining inner cells a chance to finally contact the ectoderm.

The resolution of mesodermal cell behaviour described here will make it possible to analyse in greater detail the migration defects in mutants such as *htl* and *pebble*. It will also make it possible to test whether cell rearrangements are normal in those situations in which directional information is lost, but in which spreading still occurs (e.g. rescue with activated Htl, or widespread, non-localised expression of FGF ligands). Finally, it will be of interest to determine whether the behaviours we have observed are typical of mesoderm migration in other systems. In mouse embryos, mesodermal cells emanating from the primitive streak migrate out over the basal surface of the primitive ectoderm to eventually form the mesodermal layer of cells (Tam and Behringer, 1997). The cell rearrangements that occur during this process are not known. Photoactivatable GFP, which has provided such a versatile analysis tool here, could be applied to cultured mouse embryos to resolve these events.

**Supplementary material**

**References**
**Beiman, M., Shilo, B. Z. and Volk, T.** (1996). Heartless, a Drosophila FGF receptor homolog, is essential for cell migration and establishment of several mesodermal lineages. *Genes Dev.* **10**, 2993-3002.
**Gisselbrecht, S., Skeath, J. B., Doe, C. Q. and Michelson, A. M.** (1996). heartless encodes a fibroblast growth factor receptor (DFR1/DFGF-R2) involved in the directional migration of early mesodermal cells in the Drosophila embryo. *Genes Dev.* **10**, 3003-3017.
**Grieder, N. C., de Cuevas, M. and Spradling, A. C.** (2000). The fusome organizes the microtubule network during oocyte differentiation in Drosophila. *Development* **127**, 4253-4264.
**Gryzik, T. and Muller, H. A.** (2004). FGF8-like1 and FGF8-like2 encode putative ligands of the FGF receptor Htl and are required for mesoderm migration in the Drosophila embryo. *Curr. Biol.* **14**, 659-667.
**Imam, F., Sutherland, D., Huang, W. and Krasnow, M. A.** (1999). *stumps*, a Drosophila gene required for Fibroblast Growth Factor (FGF)-directed migrations of tracheal and mesodermal cells. *Genetics* **152**, 307-318.
**Leptin, M.** (2005). Gastrulation movements: the logic and the nuts and bolts. *Dev. Cell* **8**, 305-320.
**Lin, X., Buff, E. M., Perrimon, N. and Michelson, A. M.** (1999). Heparan sulfate proteoglycans are essential for FGF receptor signaling during Drosophila embryonic development. *Development* **126**, 3715-3723.
**Maddox, A. S. and Burridge, K.** (2003). RhoA is required for cortical retraction and rigidity during mitotic cell rounding. *J. Cell Biol.* **160**, 255-265.
**Michelson, A. M., Gisselbrecht, S., Buff, E. and Skeath, J. B.** (1998). Heartbroken is a specific downstream mediator of FGF receptor signalling in Drosophila. *Development* **125**, 4379-4389.
**Patterson, G. H. and Lippincott-Schwartz, J.** (2002). A photoactivatable GFP for selective photolabeling of proteins and cells. *Science* **297**, 1873-1877.
**Post, J. N., Lidke, K. A., Rieger, B. and Arndt-Jovin, D. J.** (2005). One- and two-photon photoactivation of a paGFP-fusion protein in live Drosophila embryos. *FEBS Lett.* **579**, 325-330.
**Roote, C. E. and Zusman, S.** (1995). Functions for PS integrins in tissue adhesion, migration, and shape changes during early embryonic development in Drosophila. *Dev. Biol.* **169**, 322-336.
**Schumacher, S., Gryzik, T., Tannebaum, S. and Muller, H. A.** (2004). The RhoGEF Pebble is required for cell shape changes during cell migration triggered by the Drosophila FGF receptor Heartless. *Development* **131**, 2631-2640.
**Smallhorn, M., Murray, M. J. and Saint, R.** (2004). The epithelial-mesenchymal transition of the Drosophila mesoderm requires the Rho GTP exchange factor Pebble. *Development* **131**, 2641-2651.
**Stark, D. A. and Kulesa, P. M.** (2005). Photoactivatable green fluorescent protein as a single-cell marker in living embryos. *Dev. Dyn.* **233**, 983-992.
**Stathopoulos, A. and Levine, M.** (2004). Whole-genome analysis of Drosophila gastrulation. *Curr. Opin. Genet. Dev.* **14**, 477-484.
**Stathopoulos, A., Tam, B., Ronshaugen, M., Frasch, M. and Levine, M.** (2004). pyramus and thisbe: FGF genes that pattern the mesoderm of Drosophila embryos. *Genes Dev.* **18**, 687-699.
**Tam, P. P. and Behringer, R. R.** (1997). Mouse gastrulation: the formation of a mammalian body plan. *Mech. Dev.* **68**, 3-25.
**Vincent, S., Wilson, R., Coelho, C., Affolter, M. and Leptin, M.** (1998). The Drosophila protein Dof is specifically required for FGF signaling. *Mol. Cell* **2**, 515-525.
**Wilson, R. and Leptin, M.** (2000). Fibroblast growth factor receptor-dependent morphogenesis of the Drosophila mesoderm. *Philos. Trans. R. Soc. Lond. B Biol. Sci.* **355**, 891-895.
**Zacharias, D. A., Violin, J. D., Newton, A. C. and Tsien, R. Y.** (2002). Partitioning of lipid-modified monomeric GFPs into membrane microdomains of live cells. *Science* **296**, 913-916.